

Multibody interactions lead to conformational selection of an open state in warm GABA_A receptors

Sruthi Murlidaran^{a,1}, Reza Salar^{a,b,2}, and Grace Brannigan^{a,b,3}

^aRutgers University, Center for Computational and Integrative Biology, Rutgers University, Camden, NJ, USA; ^bDepartment of Physics, Rutgers University, Camden, NJ, USA

γ_2 GABA_A receptors are critical for proper transmission of inhibitory signals in the central nervous system, and are common targets of anesthetic and anxiolytic drugs. They are also members of the widely-studied pentameric ligand-gated ion channel family (pLGIC). Here we use a slightly increased temperature to, for the first time, observe a stable spontaneous opening event of a pLGIC in molecular simulation. We find the opening event reflects interactions in two rings of homologous charges in the receptor transmembrane domain, an "interfacial band" containing five basic residues at M2 24' in the M2-M3 loop, and the "pore oscillator" composed of two acidic residues and one basic residue at 20' on the two β and one γ M2 helices respectively. The pore oscillator is shown to drive fluctuations in pore radius, by switching between attractive and repulsive cross-pore electrostatic interactions, consistent with a classic Coulomb charge-dipole arrangement. A conformational change of the interfacial band from an asymmetric to a symmetric state locks the pore oscillator in a repulsive (open) configuration. The γ_2 K289M mutation is a rare mutation (rs121909672) that causes seizures with fever and also neutralizes the γ_2 residue in the interfacial band. The electrostatic energy of an interfacial band with only four charges is shown to be more sensitive to random shape fluctuations, which increase with higher temperature. Our simulation results indicate these effects are also transmitted to the pore. Temperature-enhanced fluctuations could thus cause rapid gating in these mutant receptors, consistent with flickering observed previously in single-channel recordings.

Gamma-aminobutyric acid (GABA_AR) receptors are inhibitory ionotropic receptors, critical to proper function of the mammalian central nervous system (CNS) and targets of numerous drugs aiming to depress CNS activity, such as benzodiazepines(1), and inhalational and intravenous general anesthetics.(2–4) They are members of the well-studied family of pentameric ligand-gated channels (pLGICs), which includes several other receptors common to CNS membranes, such as the nicotinic acetylcholine receptor (nAChR), 5HT-3 receptor, and glycine receptor. The larger family is found in a range of organisms, including prokaryotes, and exhibits high sequence and function diversity. Surprisingly, high resolution x-ray structures have revealed a common structure that is extremely well-conserved across the family, (5–14) which has made it particularly challenging to identify a universal group of interactions that drive gating.

Molecular simulation is a powerful technique for identifying subtle differences in interactions. It has been unfeasible to directly observe transitions to stable open states even in long molecular simulations of pLGICs, and pLGIC open state structures reliably close upon unbiased simulation, even under

conditions in which they're expected to be stable. (15–18) Identifying opening pathways, therefore, requires an artificial bias or selection process to drive the receptor toward an open conformation. The pH-sensitive prokaryotic pentameric GLIC channel has been crystallized at high resolution in multiple conformations, and at pH corresponding to both resting and active states,(9–11); probable pathways between conformations have been determined using increasingly sophisticated molecular dynamics algorithms.(19–22) Such studies have identified collective motions common to the gating pathway, with Lev et al(22) recently identifying a sequence of collective events common to pathways generated using an enhanced sampling technique known as the string method.

The underlying origins of this instability have not been identified despite extensive efforts, in part because identifying the essential interactions missing from the simulation requires answering *a priori* the primary question the simulations hope to address : which interactions drive pore opening and closing. Simulations of gating in neurotransmitter-gated pLGICs are further hampered by low orthosteric ligand binding affinity due to a loss of cation- π interactions in non-polarizable forcefields.

Here we circumvent both these obstacles by exploiting the allosteric properties of pLGICs. In a classic Monod-Wyman-Changeux(23, 24) model of allostery, unliganded receptors still fluctuate between active and resting conformations, with the probability of the active conformation usually expected to increase with small temperature increases. We observe conformational shifts consistent with the events at the domain interface reported by Lev et al(22), but are able to further identify the sequence of events preceding the spontaneous

Significance Statement

GABA(A) receptors are neurotransmitter receptors that inhibit electrical signals in the brain and are necessary to prevent seizures. They are also targets of inhibitory drugs, like sedatives and general anesthetics. Some GABA(A) mutations increase the likelihood of seizures, but only with fever, and can be found in humans. We use Molecular Dynamics Simulations to explore the effects of temperature and one such mutation on virtual GABA(A) receptors, and newly identify a set of interactions that both allows gating of Wild-type receptors and mediates the temperature effects of the mutation. This opens new doors for interpreting complex experimental results, predicting effects of amino-acid sequence on GABA(A) receptor function and other proteins in the same family, and design of anti-convulsant drugs.

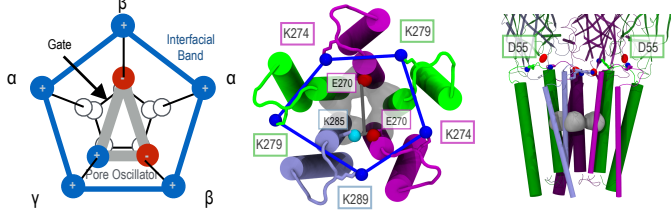


Fig. 1. (A)Schematic of the GABA_AR pore with relevant multibody interactions. A conserved basic residue at 24' in the M2-M3 loop forms a pentamer of positive charges, interfacial band, drawn here in blue. The γ K289M mutation neutralizes one of the charges. One turn closer to the intracellular domain, one basic residue and two acidic residues constitute a charge-dipole arrangement, pore oscillator, is shown in gray. The tightest constriction is at the hydrophobic gate at 9', lined by five leucines (white). (B) View of the TMD from ECD, colored by subunit; γ - iceblue; β - purple; α - green. Charged ends of the residues forming the interfacial band and pore oscillator are represented by spheres connected (for visualization only) by gray and blue bonds respectively. Space-filling representation in gray depicts the hydrophobic gate at 9'. (C) Side view of ECD and TMD showing the residues in (B), as well as the position of α D55 in the ECD.

pore opening, as well as the collective electrostatic interactions that drive them.

Each pLGIC subunit consists of an extracellular agonist-binding domain (ECD) and a transmembrane domain (TMD) containing a four helix bundle with helices labeled (M1-M4). The M2 helices line the pore, and the M2-M3 loop connecting the M2 and M3 helices interacts directly with both the TMD and the ECD. The loop has long been hypothesized to transmit agonist binding to the transmembrane domain,(25–30) with several mutation studies indicating the importance for agonist sensitivity of attractive electrostatic interactions among contact residues, such as salt-bridges, between the M2-M3 loop and the ECD. (31–34) The mechanism through which a change in these salt bridges (either forming or breaking) opens the pore is still unclear.

Our results suggest a non-specific mechanism for the final steps of gating that relies on multibody interactions within two sets of homologous charged residues: 1) a group of three residues containing both positive and negative charges, facing into the pore and forming a rapidly oscillating charge-dipole arrangement, which we term the pore oscillator, and 2) an interfacial band of five like charge residues at the interface of the ECD and TMD which, upon an energetically unfavorable conformational change, selects for an open conformation of the pore oscillator(Figure 1).

We show using simple electrostatic expressions that repeated cross-pore repulsions in the interfacial band introduce a significant energetic penalty for shrinking the interfacial band, and that the symmetry inherent in the interfacial band amplifies the interactions between distant residues. Molecular dynamics simulations indicate this repulsion among interfacial band residues can be propagated along M2 helices to open the hydrophobic gate. In GABA_AR receptors, the interfacial band is formed by a basic residue in the M2-M3 loop conserved across GABA_AR subunits as α K279, β K274, or γ K289 (Figure 1), and notated as M2 24' in the prime numbering scheme suggested in (35). Sequence conservation of these charges across GABA_AR subspecies is shown in Figure S3. M2 24' has been previously shown to be critical for conferring sensitivity to agonist; Harrison and colleagues(33) demonstrated via

shift in EC50 that charge-reversal of α 279 reduced sensitivity, which was restorable via additional charge-reversal of α D57 or α D149, both within the ECD and in the vicinity of the M2-M3 loop. Similar behavior was observed in the nicotinic acetylcholine receptor (nAChR), upon charge-reversal of α R209 in M1 and α E45 in the ECD.(28)

The basic residue at M2 24' is also conserved in GLIC, ELIC, and GlyR, and was further implicated in interdomain communication in simulations of GLIC by Lev et al(22), who also found that salt bridging of M2 24' with the ECD (D32) is correlated on a “high-probability communication pathway” with shrinking distances between M2 helices and pore closure. A causative and predictive physical mechanism, however, was not established.

Negative effects of a natural but uncommonly occurring missense single nucleotide polymorphism (SNP) at M2 24' in the γ_2 subunit supports a role for collective charge interactions in stabilizing the open state. The γ_2 :K289M mutation has been reported in families with generalized epilepsy and febrile seizures plus(GEFS+)(36–38), a generalized phenotype that often includes only febrile (fever-caused) seizures until about age 11, but can also include less severe myoclonic, atonic, or absence seizures at normal body temperature. In $\alpha_1\beta_2\gamma_2$ K289M receptors, GABA-evoked current amplitude was dramatically reduced relative to the WT (37, 39), while in $\alpha_1\beta_3\gamma_2$ K289M receptors the mutation did not affect current amplitudes but did increase the deactivation rate(40). In the latter receptors, currents had reduced mean open times, in part due to flickering(34, 38, 41). In hippocampal neurons containing GABA_AR with γ_2 :K289M subunits, accelerated desensitization of inhibitory post synaptic currents was also observed(40). Although a mechanism involving reduced trafficking has been proposed,(42) this would not explain the flickering observed in single-channel recordings.(38)

We have run unbiased MD simulations and adaptive biasing force (ABF) calculations of the γ K289M mutant at multiple temperatures, and detect occluded channels at higher temperatures consistent with the known behavior of the K289M mutants, with differential dynamics of the interfacial band consistent with expectations based on the multibody expression. We propose a mechanism underlying the mutation's effects, involving destabilization of the open state due to the reduced cost to shrink a interfacial band with significant shape fluctuations .

MATERIALS AND METHODS

Simulations. This manuscript considers data from four systems: two replicas of the wildtype $\alpha_1\beta_1\gamma_2$ receptor (termed K1, K2) and 2 replicas of the K289M mutant (M1, M2). Each system was run for 500 ns at both 300K and 315K, for a total of 4 μ s of unbiased MD simulation. Additional free energy calculations involved the K1 and M1 systems.The model used in this paper corresponds to Model 1 - CHOL from Reference(43), and was built with GluCl (PDB code : 3RHW) as a template as well as the alignments published in Ref(44). Further justification and details on this model can be found in Reference(43). The systems were prepared as in Ref(43), by embedding the protein in a lipid bilayer composed of 4:1 phosphatidylcholine (POPC) : cholesterol mixture built using CHARMM Membrane builder, with the final system containing 266 POPC molecules. All simulations used the

249 CHARMM22-CMAP(45) force field with torsional corrections
 250 for proteins. The CHARMM36 model(46, 47) was used for
 251 phospholipids, ions, water and cholesterol molecules. Energy
 252 minimization and MD simulations were conducted using the
 253 NAMD2.9 package(48). A cutoff of 1.2 nm was used for non-
 254 bonded potentials, with a switching function starting at 1.0
 255 nm; all simulations employed periodic boundary conditions,
 256 and long-ranged electrostatics were handled with smooth Par-
 257 ticle Mesh Ewald method with a grid spacing of approximately
 258 1Å. All simulations were run in the NPT ensemble with weak
 259 coupling to Langevin thermostat at temperature 300 or 315K,
 260 and a Langevin barostat at 1 atm. High temperature (315K)
 261 simulations were run for 500 ns following 200 ns of simulation
 262 at the lower temperature (300K). Full details are provided in
 263 SI.
 264

265 **Analytical Prediction of Multibody Interactions.** Our simula-
 266 tion analysis is motivated by the multibody interactions within
 267 two arrangements of charges found around the GABA(A)r
 268 pore, representing the interfacial band and the pore oscillator.
 269 Each arrangement includes residues on opposite sides of
 270 the pore, and the plane containing the residues is normal to
 271 the pore axis, so attractive and repulsive interactions within
 272 the arrangement will contribute directly to pore-closing and
 273 pore-opening, respectively.
 274

275 **Charged pentamer.** As shown in SI Theory, the total Coulomb
 276 energy for a charged pentagon with average side length \bar{r} and
 277 average diagonal length \bar{s} is
 278

$$279 \quad U_{+5}(\bar{r}, \delta_\phi) = \frac{5k_e e^2 \phi}{\bar{r}} \left(1 + \frac{\delta_\phi}{\phi} \right) + O(\bar{r}^2) + O(\bar{s}^2) \quad [1]$$

280 where e is the electron charge, $k_e = 332\text{Å}/\text{kcal/mol}/e^2$ is the
 281 Coulomb constant, and \bar{r}^2 and \bar{s}^2 are the variance in r and
 282 s across the five sides of the pentamer. For a regular pentamer
 283 $\bar{s} = \phi \bar{r}$ where $\phi \equiv (1 + \sqrt{5})/2 \sim 1.62$ is a geometric constant
 284 often called the “golden ratio”, with the convenient property
 285 $1/\phi = \phi - 1 = 0.62$. δ_ϕ is the deviation of \bar{r} from the value
 286 for a regular pentamer : $\delta_\phi \equiv \bar{r} - (\phi - 1)$.
 287

288 The linear term in δ_ϕ reflects the effects of shape fluctua-
 289 tions on the relative contributions of diagonal and adjacent
 290 pairs. Second-order terms given by \bar{r}^2 and \bar{s}^2 reflect variance
 291 in the adjacent and diagonal distances respectively. According
 292 to Eq. 1, positive values of δ_ϕ (in which diagonal distances are
 293 shorter than expected in a regular pentamer) will increase the
 294 overall energy of the interfacial band, provided the average
 295 distance between adjacent residues (\bar{r}) is kept constant. This
 296 asymmetry-induced increase in energy can be offset by an
 297 overall increase in the size of the interfacial band : $\delta_\phi > 0$ will
 298 stabilize a larger \bar{r} . Similarly, negative δ_ϕ will decrease the
 299 overall energy of the interfacial band and allow it to close with
 300 reduced penalty.
 301

302 Neutralizing any of the charges removes two diagonal and
 303 two adjacent interactions, so the Coulomb energy for 4 like-
 304 charges arranged on a pentagonal lattice is
 305

$$307 \quad U_{+4}(\bar{r}, \delta_\phi) = \frac{3k_e e^2 \phi}{\bar{r}} \left(1 + \frac{\delta_\phi}{\phi} \right) + O(\bar{r}^2) + O(\bar{s}^2) \quad [2]$$

$$309 \quad = \frac{3}{5} U_{+5}(\bar{r}, \delta_\phi) \quad [3]$$

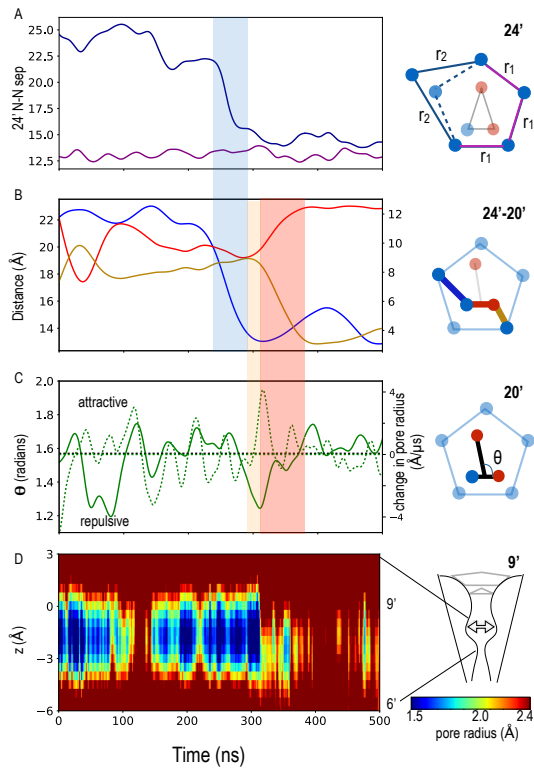


Fig. 2. Evolution of the interfacial band and pore oscillator in one replica of the WT system at 315K. (A) Flip of one residue (α -K279) so the interfacial band switches from elongated to regular pentamer, occurs at ~ 250 ns, followed by a series of events leading to the pore opening between ~ 250 ns - ~ 350 ns, as marked by the shaded regions. (B) The distances between residues α K279 – γ K285, plotted on y-axis and γ K285 – β -K270, β -K270 – β -K274, plotted on alternate y-axis, are shown in blue, red and gold respectively. (C) The solid green curve depicts the angle between the charge-dipole arrangement representing the pore oscillator ; The Dotted green line represents the pore-opening event as measured by calculating the first derivative of the minimum pore radius. (D) Pore radius as a function of distance along the pore axis and time. All curves are smoothed as described in SI Methods. Transition windows are shaded blue (early), orange (mid), and red (late).

351 where averages only consider distances involving charged
 352 residues, and therefore \bar{r} and δ_ϕ incorporate only three adja-
 353 cent distances and three diagonal distances. The factor of $3/5$
 354 will generally stabilize a smaller value of \bar{r} at any temperature,
 355 but $\delta_\phi, \bar{r}^2, \bar{s}^2$ will also be directly dependent on temperature.
 356 The simple Coulomb calculation represented in Eq. 1 indicates
 357 a large energetic cost of shrinking the interfacial band over typi-
 358 cal distances (Fig S1B). Considering typical distances between
 359 homologous residues in pLGICs, the strength of the interaction
 360 among homologous residues may be unintuitive. Reducing the
 361 distance between two like charges from $r_1 = 15\text{Å}$ to $r_1 = 12\text{Å}$
 362 raises the electrostatic energy by only 5.5 kcal/mol, but shrink-
 363 ing the regular pentagon (including diagonal interactions) from
 364 $r_1 = 15\text{Å}$ to $r_1 = 12\text{Å}$ increases the energy of the arrangement
 365 by 49 kcal/mol! Diagonal, cross-pore interactions contribute
 366 almost 20 kcal/mol, nearly doubling the total.
 367

Charge-dipole. Farther away from the interface with the ECD, facing the pore, is another charged ring of three residues, at M2 20' (β E270 and γ K285), that we term the “pore oscillator” because it exhibits rapid shape fluctuations that are propa-
 368
 369
 370
 371
 372

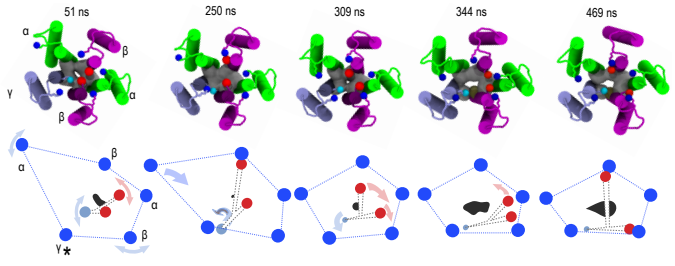


Fig. 3. Evolution of pore oscillator and interfacial band during spontaneous opening event. Top: Representative frames are shown from the WT trajectory at 315K, with coloring as in Figure 1B/C. Bottom: Cartoon of transition highlighting movement of the charged groups forming interfacial band(blue) and pore oscillator (γ K280-cyan, β E270-red). Dashed lines connecting the points of the pore oscillator and interfacial band are for visualization purposes only and do not represent physical bonds. The filled gray shape indicates the unoccluded area of the hydrophobic gate. After α K279 flips during the symmetrization step, M2 helices separate along the axis connecting the flipped and current positions (frame at 344 ns), while after the acidic residues pivot, M2 helices separate along the axis connecting the two acidic residues (post-transition panel). Salt-bridges are represented by contacting red and blue spheres. The asterisk marks the charge that is neutralized with the K289M mutation.

gated to the hydrophobic gate. The Coulomb energy reflects two diagonal interactions, and one adjacent interaction, and is effectively a charge-dipole interaction:

$$U_{c-dp} = -\frac{k_e e^2}{r} \left(\frac{r}{d} + \frac{1}{z^+} - \frac{1}{z^-} \right) \quad [4]$$

$$z^\pm \equiv \sqrt{1 + \left(\frac{d}{2r} \right)^2 \pm \frac{d \cos \theta}{r}} \quad [5]$$

where U_{c-dp} is the Coulomb energy of the charge-dipole, d is the distance between the two charges forming the dipole, r is the separation between the charge and dipole midpoint, z^\pm are the distances between the charge and the close and far ends of the dipole, respectively, and θ is the angle between the dipole and dipole midpoint-charge separation vector (see diagrams in Fig. 3C and S1B).

It is common in undergraduate-level treatment of charge-dipole interactions to assume $r/d >> 1$ in Eq. 4, but for a charge-dipole arranged on a regular pentagonal lattice, $r/d \equiv \phi \sim 1.6$. One central result from the usual treatment is that at $\theta = \pi/2$, the interaction switches from being attractive to repulsive, with a discontinuity at the boundary; this result still holds in the full expression (Fig S1B), as expected.

RESULTS AND DISCUSSION

Spontaneous opening event at 315 K. A spontaneous opening event was observed in one WT replica at the higher temperature. In this replica, the pore was closed for over 500 ns at 300K (Figure S6), but after raising the temperature to 315K and about 200 ns of simulation, a spontaneous set of events induced a stable open pore for the remainder of the simulation. (Figure 3, and SI Movie S1). The event itself took about 100-150 ns, and involved the following stages, shaded by the specified colors in Figure 3.

1. Early (blue): Symmetrization of interfacial band.

The interfacial band begins in an elongated conformation, because the side-chain of one charged residue (α_γ -K279)

faces away from the pore axis, while all other side-chains face toward it. Between 200 and 260 ns, this side-chain flips, causing the interfacial band to switch from an elongated to a regular conformation (Figure 2 A). This flip may be dependent upon flexibility introduced by the adjacent proline (α P278); the conservation(35) and significance of this proline for function(27) are well-established, although its fundamental role in gating has been unclear.

2. Mid (orange): Response to symmetrization; partial opening and deformation.

- (a) t = 260-300 ns: The previous symmetrization step is electrostatically unfavorable for the other residues of the interfacial band and for the basic residue of the pore oscillator; in response, the M2 helices of the flipped α subunit and the γ and β subunit on either side separate from the other two subunits. This initiates widening of the pore, as shown by the sharp transition in Figure 2 D. Simultaneously, the positively-charged end of the pore oscillator dipole (γ -K285) is deflected toward the intracellular domain and away from the ECD (Figure 3). This destabilizes its salt-bridge with the negatively charged residue comprising the other end of the “dipole”, β_γ -E270.
- (b) t=300-330 ns: Upon weakening of favorable electrostatic interactions with positively charged residues in the pore oscillator and interfacial band, the two negative sidechains of the pore oscillator pivot around their C_α atom to face away from the γ subunit. This switches the pore oscillator charge-dipole interaction from attractive to repulsive, as tracked by θ in Figure 3 C and according to Eq. 4; for small values of θ , the distance between the two negatively charged residues becomes particularly small (Figure 3).

3. Late (red): Recoil and Stabilization.

The pore-oscillator is now in a highly unfavorable configuration due to proximity of the two negative charges corresponding to low values of θ . The resulting repulsion causes a rapid separation of the charges. This is further propagated to increase the distance between their respective M2 helices, as indicated by an additional increase in pore radius, not just at the pore oscillator but also at the minimum constriction 16-17 Angstroms away (Figure 2 D). The trajectories of θ and the time derivative of the minimum pore constriction are shown plotted on the same axis in Figure 2 C; the two most rapid increases in the pore radius each occur directly after the two θ compression events (at t = 100 ns and t = 325 ns). This association was also qualitatively observed in the other replica trajectories (Figures S5-S11), although in some cases it was a less acute value of θ , held over a longer time period, that preceded opening.

Upon recoil, each of these two acidic residues formed an intrasubunit salt-bridge with a basic residue of the interfacial band (Figure 2 B). Since the charged interfacial band is resistant to shrinking, these salt-bridges can only form if the acidic residues in the pore oscillator are also separated. The timing of events is consistent with pore oscillator recoil simultaneously allowing salt-bridging with

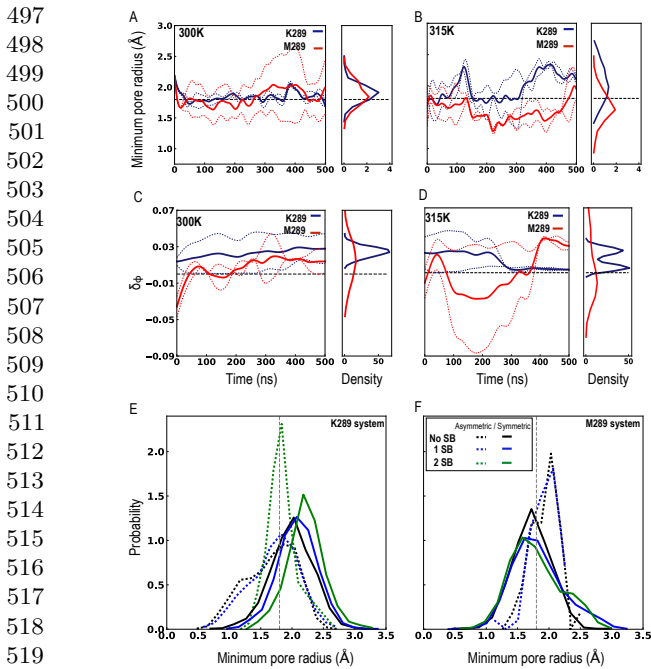


Fig. 4. Correlations between shape of interfacial band, pore radius, and salt-bridging between interfacial band and pore oscillator for multiple replicas and temperatures. (A/B) Smoothed time evolution of the pore minimum constriction, averaged (solid 521 lines) over two replicas (shown separately as dotted lines) each, at 300 K and 315 K. 522 The radius of a chloride ion is represented by the dashed horizontal line at 1.8 Å. (C/D) 523 Smoothed time evolution and distribution of δ_ϕ for both WT and K289M systems at 300 524 and 315 K. Distribution trends are similar to those generated numerically, discussed 525 in SI Theory. (E/F) Distribution of minimum constriction radius for conformations 526 clustered by total number of β -K274-E270 salt-bridges and symmetrization of the 527 interfacial band.

the interfacial band and causing an overall separation of M2 helices. Due to the stochastic nature of the trajectory, determining the typical order of these two events would require many more replicas.

The pore oscillator samples small values of θ regardless of the configuration of the interfacial band, due to high frequency oscillations consistent with the discontinuity in the interaction, including twice in this particular trajectory (once at $t = 100$ ns and once at $t = 350$ ns). Such events were observed in all simulated systems and were usually followed by brief opening of the pore. A stable opening event, however, was only observed when salt-bridging of each of the pairs of β -E270 and β -K274 residues was also stable, which depended upon the symmetrization step. The significance of the symmetric interfacial band is verified through the next set of simulations involving a mutant of an interfacial band residue.

γ K289M increases energetic sensitivity to shape fluctuations of the interfacial band. The multibody mechanism proposed in the previous section suggests an important role for each basic residue in the interfacial band for conferring stability of the open state, beyond communication with the agonist-binding domain. γ subunits are not required for functional GABA(A) receptors, and do not participate in the interfaces forming the orthosteric binding sites. Yet neutralizing the γ -contributed charge to the interfacial band causes flickering in single-channel recordings (38) and is associated with fever-induced seizures.

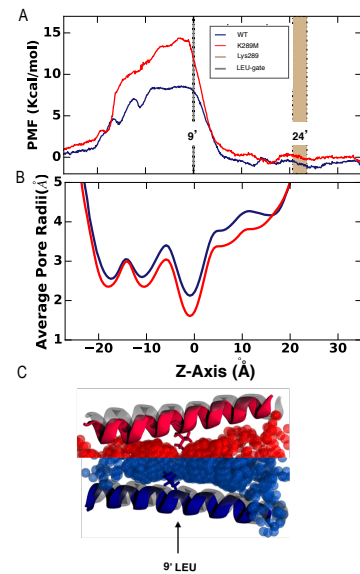


Fig. 5. (A) Potential of mean force profile of a chloride ion crossing the ion channel, calculated at 315 K for a receptor that remained primarily in the elongated conformation for the WT and had a flexible interfacial band for the K289M. The full PMF including the rest of the simulation box is in Fig S14. (B) Average pore radius profile for the conformations in (C).

Simulations of the two K289M replicas at both 300 K and 315 K, as for the WT receptors, indicated a reverse temperature dependence for the distribution of minimum pore radii (Figure 4). As shown in Figure 4 A, we observe no effect of the mutation on the overall distribution of pore radii at 300 K. At 315 K, the WT distribution broadens, as expected (Figure 4 B). The K289M distribution broadens even more at the higher temperature, but is also shifted toward smaller radii, so that at 315 K both WT replicas have larger pore radii than both K289M replicas for most frames.

Eq. 3 indicates three possible contributions to a reduced cost for shrinking the K289M interfacial band compared to that of the WT interfacial band:

1. The reduced charge of the K289M interfacial band results in a factor of 3/5 for the overall energetic cost to shrink the K289M interfacial band, assuming the same value of \bar{r} and δ_ϕ . This contribution is not temperature dependent, and the 40% loss is large enough that it is perhaps most surprising that an K289M receptor is functional at any temperature. This may be explained by the observation that in the K289M systems, $\gamma M220'$ (M2 K285) of the pore oscillator assumes a position much closer to the original position of K289.
2. Any reduction in δ_ϕ will destabilize the open state by reducing the energetic cost to shrink the interfacial band (Eq. 1). Both increased temperature and the loss of charge symmetry would be expected to increase the root-mean-square-displacement (RMSD) of each remaining side-chain. We ran simple numerical calculations to determine how increased RMSD in individual charges affects the distribution of δ_ϕ , shown in Figure S2. The distribution of δ_ϕ is not particularly sensitive to RMSD if all five charges of a closed pentagon are used, due to geometric constraints and the non-cohesive nature of the noise. The

621	distribution is expected to widen with increased RMSD,	683
622	but mainly in the positive direction (Figure S2A).	684
623		685
624	3. Even if each individual (conserved) charge has the same	686
625	RMSD in the K289M and WT receptors, the distribution	687
626	of δ_ϕ will be broadened in the K289M receptor because	688
627	only three of the five adjacent and diagonal distances	689
628	are used to calculate the average adjacent and diagonal	690
629	distances, and they are not constrained by the requirement	691
630	of forming a closed pentagon (Figure S2). Furthermore,	692
631	the broadening is symmetric, with significant probability	693
632	of $\delta_\phi < 0$. This is consistent with what we observe in the	694
633	molecular systems, as shown by deviations of the ratio of	695
634	diagonal to adjacent distances from $1/\phi$ (Figure 4 C,D)	696
635	over each trajectory.	697
636		698
637	Comparison between Figure 4A,B and C,D, reveals similar	699
638	trends for distributions of minimum pore radius and δ_ϕ , upon	700
639	introducing the mutation, raising the temperature, or both.	701
640	The pore oscillator-interfacial band salt-bridge formation	702
641	becomes uncorrelated from the pore radius in the K289M	703
642	systems, as shown in Figure 4 F.	704
643		705
644	γ K289M increases barriers to conduction via channel confor-	706
645	mination rather than direct interactions with ions. Determining	707
646	whether a single ion channel conformation corresponds to an	708
647	"open" or "closed" state is frequently not possible in unbiased	709
648	MD simulations, except for conformations at an extremum. A	710
649	Cl- atom has a radius of approximately 1.8 Å, the hydrophobic	711
650	residues lining the minimum pore radius but makes it unlikely	712
651	a Cl- atom will pass through a constriction of exactly 1.8 Å ;	713
652	when both salt bridges between the interfacial band and pore	714
653	oscillator are formed, the WT receptor has a minimum pore	715
654	radius of at least 2.5 Å .	716
655	The effects of the mutation on purely electrostatic barriers	717
656	for chloride ion translocation was quantified via the Poisson-	718
657	Boltzmann equation as described in SI Methods. The mutation	719
658	from a positively charged to neutral residue led to insignificant	720
659	changes in the electrostatic potential along the most favorable	721
660	path given identical starting conformations (as shown in Sup-	722
661	plementary Figure S12), suggesting that the mutation alone	723
662	could not affect conductance without inducing conformational	724
663	shift. Although the electrostatic potential is weakened near	725
664	the mutation, the ion can adjust its pathway through the	726
665	channel to fall closer to the other four residues in the interfa-	727
666	cial band. Calculation of the electrostatic potential using the	728
667	equilibrated structures of WT and K289M receptors showed	729
668	a 5-10 kcal/mol (Figure S12C) higher electrostatic barrier	730
669	in K289M, predominantly occurring in the transmembrane	731
670	domain enclosing the residues containing the minimum pore	732
671	constriction region.	733
672	The PMF for chloride ion translocation at 315K, measured	734
673	using ABF, is shown in Figure 5. The largest barrier for the	735
674	WT of 8 kcal/mol is proximal to the leucine residues at M2	736
675	9', forming the tightest constriction; this barrier is increased	737
676	by 5 kcal/mol for the mutant receptors. The difference in	738
677	PMF near residue γ_2 289 is much less than 1 kcal/mol. While	739
678	mutation of a positively charged to neutral residue does have	740
679	a small effect on affinity of the chloride ion for the region of	741
680	the receptor near the mutation, the dominant effect of the	742
681	mutation on conduction is via conformational instability of	743
682	the open state.	744
621	CONCLUSION	683
622	The primary new insights of this work are:	684
623		685
624	1. Repulsive cross-pore electrostatic interactions at the	686
625	TMD-ECD interface (the "interfacial band") stabilize	687
626	the open state of the GABA(A) receptor; the interfacial	688
627	band becomes more resistant to shrinking as the average	689
628	separation between adjacent charges decreases or as the	690
629	relative strength of diagonal interactions is reduced.	691
630		692
631	2. In GABA _A R receptors with 2 α subunits, 2 β subunits,	693
632	and 1 γ subunit, a three-body charge-dipole arrangement	694
633	(the "pore oscillator") among three M2 helices (two ad-	695
634	jacent and one diagonal) drives fluctuations in minimum	696
635	pore radius, by alternating between a repulsive and an	697
636	attractive configuration. All three charges are conserved	698
637	within α , β and γ species of the GABA(A) receptor (al-	699
638	though γ_3 has an arginine instead of a lysine, Figure	700
639	S3).	701
640		702
641	3. Switching from an asymmetric to symmetric configuration	703
642	of the interfacial residues in (1) can lock the charge-dipole	704
643	interaction in (2) in a repulsive configuration, via a pair	705
644	of salt-bridges between the pore oscillator and interfacial	706
645	band.	707
646		708
647	4. Neutralizing one of the residues from (1), as in the	709
648	epilepsy-associated γ_2 K289M mutations, makes the cost	710
649	to shrink the interfacial band more sensitive to dispersion	711
650	of the remaining charges; at higher temperatures this	712
651	results in a significant population of closed states. This is	713
652	consistent with the flickering observed in receptors with	714
653	this mutation in <i>vitro</i> , as well as the critical role of fever	715
654	in inducing seizures for this phenotype.	716
655		717
656	The debate over the mechanism through which binding of	718
657	a ligand at one site regulates the effects of binding of a ligand	719
658	at another site ("allostery") is over fifty years old,(23, 24) and	720
659	much of that debate was focused on placing mechanisms within	721
660	two extreme cases : "conformational selection" (functional	722
661	conformations are visited in the absence of ligand but stabilized	723
662	by ligand, the Monod-Wyman-Changeux or MWC model) or	724
663	"induced fit" (functional conformations require all ligands to be	725
664	bound, also known as the Koshland-Nemethy-Filmer model).	726
665		727
666	The mechanism for pore opening observed here fits most	728
667	consistently with an MWC model, but the presence of both	729
668	the interfacial band (1) and the pore oscillator (2) suggests	730
669	a sequence of conformational events, with each event in the	731
670	sequence falling at a different location along the continuum	732
671	between pure conformational selection and pure induced fit. Al-	733
672	though effects of the substitutions of interfacial band residues	734
673	have been studied numerous times, we are unaware of mu-	735
674	tagenesis studies involving either of the residues of the pore	736
675	oscillator (γ K/R285 and β E270). The present simulation re-	737
676	sults suggest a role for these residues in determining receptor	738
677	kinetics, including desensitization.	739
678		740
679	Our results indicate that a topological view of pLGICs	741
680	may be counterproductive for conceptualizing gating mech-	742
681	anisms, because interactions entirely within a helix/subunit	743
682	(or between two adjacent helices/subunits) are only indirectly	744
621	related to conformation of the pore. While we present these	745
622	results in heteropentamers, and the presence of the pore osci-	746
623	lator requires multiple subunit species, the role of symmetry	747

745 in stabilizing conformations with open or occluded pores has
746 been demonstrated previously in both heteropentamers such
747 as nAChR(49) and homopentamers such as GLIC. (50) Our
748 results indicate a critical role for diagonal interactions in de-
749 termining the effects of asymmetry; asymmetry that decreases
750 or increases diagonal distances opens or closes the pore respec-
751 tively.

752 More generally, the Coulomb interaction between two
753 charges placed on the diagonal of a regular pentagon will
754 only be moderately reduced from the interaction they would
755 have as adjacent charges. Diagonal interactions will always
756 contribute 38% of the overall interaction energy. A role for long
757 range interactions within the nAChR TMD-ECD interface has
758 been recently demonstrated by Auerbach and colleagues(51).
759 The residues forming an interfacial band need not be located
760 in the M2-M3 loop; they could also be in the M1 linker as
761 in nAChR, or even in the M4 C-terminus. The concept of
762 an interfacial band that we propose here is topologically ab-
763 stract, but depends on pentameric symmetry and a regular
764 charge density at the interface between the two domains; it
765 may therefore be generalizable to many or even all pLGICs.
766

767 ACKNOWLEDGMENTS

768 SM, RS, and GB were supported by research grants NSF
769 MCB1330728 and NIH P01GM55876-14A1. This project
770 was supported with computational resources from the Na-
771 tional Science Foundation XSEDE program through allocation
772 NSF-MCB110149 as well as a local cluster funded by NSF-
773 DBI1126052. The authors are grateful to Dr. Jérôme Hénin
774 for multiple useful discussions.
775

1. Sigel E (1997) The benzodiazepine binding site of GABAA receptors. *Trends in Pharmacological Sciences* 18(11):425–429.
2. Krasowski MD, Harrison NL (1999) General anaesthetic actions on ligand-gated ion channels. *Cell. Mol. Life Sci.* 55(10):1278–1303.
3. Harris RA, Mihic SJ, Dilley-Mayfield JE, Machu TK (1995) Actions of anaesthetics on ligand-gated ion channels: role of receptor subunit composition. *FASEB J* 9(14):1454–1462.
4. Miller KW (2002) The nature of sites of general anaesthetic action. *Br. J. Anaesthet.* 89(1):17–31.
5. Miller PS, Aricescu AR (2014) Crystal structure of a human GABAA receptor. *Nature* 512(7514):270–275.
6. Hassaine G, et al. (2014) X-ray structure of the mouse serotonin 5-ht3 receptor. *Nature* 512(7514):276–281.
7. Du J, Lü W, Wu S, Cheng Y, Gouaux E (2015) Glycine receptor mechanism illuminated by electron cryo-microscopy. *Nature* 526(7572):224.
8. Hilf RJC, Dutzler R (2008) X-ray structure of a prokaryotic pentameric ligand-gated ion channel. *Nature* 452(7185):375–379.
9. Bocque N, et al. (2009) X-ray structure of a pentameric ligand-gated ion channel in an apparently open conformation. *Nature* 457(7225):111–114.
10. Gonzalez-Gutiérrez G, Cuello LG, Nair SK, Grosman C (2013) Gating of the proton-gated ion channel from gloeobacter violaceus at pH 4 as revealed by x-ray crystallography. *Proceedings of the National Academy of Sciences* 110(46):18716–18721.
11. Sauguet L, et al. (2014) Crystal structures of a pentameric ligand-gated ion channel provide a mechanism for activation. *Proceedings of the National Academy of Sciences* 111(3):966–971.
12. Hibbs RE, Gouaux E (2011) Principles of activation and permeation in an anion-selective Cys-loop receptor. *Nature* 474(7349):54–60.
13. Althoff T, Hibbs RE, Banerjee S, Gouaux E (2014) X-ray structures of gluc1 in apo states reveal gating mechanism of cys-loop receptors. *Nature* 512(7514):333.
14. Spurny, R. Ramerstorfer, J. Price, K. Brams, M. Ernst, M. Nury, H. Verheij, M. Legrand, P. Bertrand, D. Bertrand, S. Dougherty, D.A. De Esch, I.J.P. Corringer, P. Sieghart, W. Lummis, S.C.R. Ulens C (2012) Pentameric Ligand-Gated Ion Channel Elicits Activation by Gaba and Modulated by Benzodiazepines. *Proc.Natl.Acad.Sci.USA* 109:E3028.
15. Brannigan G, Hénin J, Law R, Eckenhoff R, Klein ML (2008) Embedded cholesterol in the nicotinic acetylcholine receptor. *Proc. Natl. Acad. Sci. USA* 105(38):14418–14423.
16. Willenbring D, Liu L, Mowrey D, Xu Y, Tang P (2011) Isoflurane Alters the Structure and Dynamics of (GLIC). *Biophys. J.* 101(8):1905–1912.
17. LeBard DN, Hénin J, Eckenhoff RG, Klein ML, Brannigan G (2012) General anesthetics predicted to block the GLIC pore with micromolar affinity. *PLoS computational biology* 8(5):e1002532.
18. Yoluk O, Brömstrup T, Bertaccini EJ, Trudell JR, Lindahl E (2013) Stabilization of the GluCl Ligand-Gated Ion Channel in the Presence and Absence of ivermectin. *Biophys J* 105(3):640–647.

19. Nury H, et al. (2010) Crystal structure of the extracellular domain of a bacterial ligand-gated ion channel. *Journal of molecular biology* 395(5):1114–27.
20. Zhu F, Hummer G (2010) Pore opening and closing of a pentameric ligand-gated ion channel. *Proceedings of the National Academy of Sciences of the United States of America* 107(46):19814–9.
21. Calmet N, et al. (2013) A gating mechanism of pentameric ligand-gated ion channels. *Proceedings of the National Academy of Sciences* 110(42):E3987–E3996.
22. Lev B, et al. (2017) String method solution of the gating pathways for a pentameric ligand-gated ion channel. *Proceedings of the National Academy of Sciences* 114(21):E4158–E4167.
23. Changeux JP, Edelstein S (2011) Conformational selection or induced fit? 50 years of debate resolved. *F1000 biology reports* 3.
24. Changeux JP, Christopoulos A (2016) Allosteric modulation as a unifying mechanism for receptor function and regulation. *Cell* 166(5):1084–1102.
25. Campos-Caro a, et al. (1996) A single residue in the M2-M3 loop is a major determinant of coupling between binding and gating in neuronal nicotinic receptors. *Proceedings of the National Academy of Sciences of the United States of America* 93(12):6118–23.
26. Grosman C, Salamone FN, Sine SM, Auerbach A (2000) The extracellular linker of muscle acetylcholine receptor channels is a gating control element. *The Journal of general physiology* 116(3):327–40.
27. Lummiss SCR, et al. (2005) Cis-trans isomerization at a proline opens the pore of a neurotransmitter-gated ion channel. *Nature* 438(7065):248–52.
28. Lee WY, Sine SM (2005) Principal pathway coupling agonist binding to channel gating in nicotinic receptors. *Nature* 438(7065):243–7.
29. Unwin N (2005) Refined structure of the nicotinic acetylcholine receptor at 4°(A) resolution. *J. Mol. Biol.* 346(4):967–989.
30. Lee WY, Free CR, Sine SM (2009) Binding to gating transduction in nicotinic receptors: Cys-loop energetically couples to pre-M1 and M2-M3 regions. *The Journal of neuroscience : the official journal of the Society for Neuroscience* 29(10):3189–99.
31. Sigel, ErwinBuhr, AndreasBaur R (1999) Role of the Conserved Lysine Residue in the Middle of the Predicted Extracellular Loop Between M2 and M3 in the GABA A Receptor. *Journal of Neurochemistry*. Oct99 73(4).
32. O'Shea SM, Harrison NL (2000) Arg-274 and Leu-277 of the gamma-aminobutyric acid type A receptor alpha 2 subunit define agonist efficacy and potency. *The Journal of biological chemistry* 275(30):22764–8.
33. Kash TL, Jenkins A, Kelley JC, Trudell JR, Harrison NL (2003) Coupling of agonist binding to channel gating in the GABA(A) receptor. *Nature* 421(6920):272–5.
34. Hales TG, et al. (2006) An asymmetric contribution to gamma-aminobutyric type A receptor function of a conserved lysine within TM2-3 of alpha1, beta2, and gamma2 subunits. *The Journal of biological chemistry* 281(25):17034–43.
35. Jaitreh M, Taly A, Hénin J (2016) Evolution of pentameric ligand-gated ion channels: Pro-loop receptors. *PLoS one* 11(3):e0151934.
36. Macdonald R (2010) Mutations in GABAA receptor subunits associated with genetic epilepsies. *The Journal of physiology*.
37. Baulac S, et al. (2001) First genetic evidence of GABA(A) receptor dysfunction in epilepsy: a mutation in the gamma2-subunit gene. *Nature genetics* 28(1):46–8.
38. Bianchi M, Song L (2002) Two different mechanisms of disinhibition produced by GABAA receptor mutations linked to epilepsy in humans. *The Journal of ...* 22(13):5321–5327.
39. Ramakrishnan L, Hess GP (2004) On the mechanism of a mutated and abnormally functioning gamma-aminobutyric acid (A) receptor linked to epilepsy. *Biochemistry* 43(23):7534–40.
40. Eugène E, et al. (2007) GABA(A) receptor gamma 2 subunit mutations linked to human epileptic syndromes differentially affect phasic and tonic inhibition. *The Journal of neuroscience : the official journal of the Society for Neuroscience* 27(51):14108–16.
41. Macdonald RL, Kang JQ, Gallagher MJ, Feng HJ (2006) GABA(A) receptor mutations associated with generalized epilepsies. *Adv Pharmacol* 54:147–169.
42. Kang JQ, Shen W, Macdonald RL (2006) Why does fever trigger febrile seizures? GABA(A) receptor gamma2 subunit mutations associated with idiopathic generalized epilepsies have temperature-dependent trafficking deficiencies. *The Journal of neuroscience : the official journal of the Society for Neuroscience* 26(9):2590–7.
43. Hénin J, Salari R, Muralidaran S, Brannigan G, Biology I (2014) A predicted binding site for cholesterol on the GABA(A) receptor. *Biophysical journal* 106(9):1938–49.
44. Hibbs RE, Gouaux E (2011) Principles of activation and permeation in an anion-selective Cys-loop receptor. *Nature* 474(7349):54–60.
45. Mackerell AD, et al. (1998) All-atom empirical potential for molecular modeling and dynamics studies of proteins. *The journal of physical chemistry. B* 102(18):3586–616.
46. Klauda JB, et al. (2010) Update of the CHARMM all-atom additive force field for lipids: validation on six lipid types. *The journal of physical chemistry. B* 114(23):7830–43.
47. Pitman MC, Suits F, Mackerell AD, Feller SE (2004) Molecular-level organization of saturated and polyunsaturated fatty acids in a phosphatidylcholine bilayer containing cholesterol. *Biochemistry* 43(49):15318–28.
48. Phillips JC, et al. (2005) Scalable molecular dynamics with NAMD. *Journal of computational chemistry* 26(16):1781–802.
49. Mitra A, Cymes GD, Auerbach A (2005) Dynamics of the acetylcholine receptor pore at the gating transition state. *Proceedings of the National Academy of Sciences* 102(42):15069–15074.
50. Mowrey D, et al. (2013) Asymmetric ligand binding facilitates conformational transitions in pentameric ligand-gated ion channels. *Journal of the American Chemical Society* 135(6):2172–2180.
51. Gupta S, Chakraborty S, Vij R, Auerbach A (2017) A mechanism for acetylcholine receptor gating based on structure, coupling, phi, and flip. *The Journal of General Physiology* 149(1):85–103.
52. Audenaert D, et al. (2006) A novel gabrg2 mutation associated with febrile seizures. *Neurology* 67(4):687–690.